Quantification of Magnetic Nanobeads With Micrometer Hall Sensors

Quantification of magnetic nanobeads with micrometer Hall sensors

Alessandra Manzin, Vahid Nabaei, and Riccardo Ferrero

***Abstract*—This paper investigates the suitability of miniaturized semiconductor Hall devices for the quantification of magnetic nanobeads usable in biomedical applications. The analysis demonstrates the existence of conditions for which the Hall voltage signal is not proportional to bead number, focusing on the detection of a 2D array of superparamagnetic nanobeads, immobilized on the sensor surface. The study is performed by means of a numerical modeling procedure, which provides the spatial distribution of the electric potential inside the Hall plate, under the assumptions of diffusive electron transport regime and non-uniform magnetic field. We find that proportionality of the sensor response to bead number and possibility to use micro-Hall devices as magnetic bead counters are strongly affected by the magnetostatic dipolar interactions between beads. We also observe a deviation from linearity, due to the spatial non-uniformity in the device response, which is strongly influenced by the planar position of the beads with respect to the device active area. These aspects are investigated in detail by varying external field amplitude, device dimension, bead number, interbead distance, bead vertical position and size of the area occupied by beads. The parametric analysis is performed simulating an ac-dc Hall magnetometry technique.**

***Index Terms*—Magnetic sensors, Micro-Hall sensors, Magnetic bead counters, Sensors for biomedical applications, Magnetic nanobeads, Magnetostatic dipolar interactions, Numerical models.**

I. Introduction

In THE VAST PANORAMA of magnetic field sensing technology, micro-Hall devices, based on semiconductor materials and, more recently, on graphene, play an important role due to their high magnetic moment sensitivity over a wide field range and elevated signal-to-noise ratio [1-3]. Additionally, they are generally characterized by a linear response, being not affected by magnetic saturation as magnetoresistive devices. These features make miniaturized Hall sensors suitable for the detection of magnetic nanobeads [4-9] used as labels for manipulating, monitoring and delivering biological species [10-11].

In the framework of Hall magnetometry, single-bead magnetic characterization was proven, reaching the detection of beads with diameter of 120-140 nm [12, 13]. Recently, nano-Hall sensors based on a nanocomposite material were successfully employed for 3D tracing of microbead position [14]. Another important result regards the mapping of the trajectory of beads moving over the sensing area of an InAs micro-Hall device, integrated into a microfluidic channel [15].

The simultaneous detection of multiple microbeads was achieved by using InSb and AlGaAs/InGaAs sensor arrays consisting of a succession of Hall probes with 5 μm size [16, 17]. An 8192 element Hall sensor array was also developed, enabling the quantification of 1% surface coverage of 2.8 μm beads [18]. Furthermore, a single sensor (an InAs double Hall cross) was successfully used for multiple detection, proving that the measured Hall resistance is proportional to the number of beads located over the active sensing area. In particular, up to 49 (resp. 9) microbeads (with 2.8 μm diameter) were simultaneously detected by means of a 20 μm (resp. 9.3 μm) width probe, showing an overall linear response [19]. These results open up the possibility of having magnetic bead counters able to measure the number of beads in proximity to the device active area and, finally, quantify the concentration of the interacting biological target in biosensing applications.

The present paper aims at analyzing the performance of micrometer semiconductor Hall devices in the detection and quantification of a high number of magnetic nanobeads. As a matter of simplicity, these are arranged in a 2D array, immobilized on the device surface. The aim is to explore conditions that cause the Hall signal to deviate from proportionality to the bead number and from linearity.

The study is performed from a modeling point of view, calculating the spatial distribution of the electric potential inside the Hall plate, under the assumptions of diffusive electron transport regime and strongly localized magnetic field. Specifically, we model the voltage response of InSb Hall probes composed of two micron-sized crosses, under the presence of an array of superparamagnetic 150 nm diameter beads located over the device active area at a fixed position. The device sensitivity is investigated referring to the ac-dc Hall magnetometry technique, which is typically employed to measure the ac variation in bead susceptibility due to a switched dc magnetic field as well as to reconstruct bead susceptibility as a function of dc field [13, 24-26].

We observe the that proportionality of the Hall signal to

Manuscript received October 03, 2018. This work was supported by Project 15SIB06 *NanoMag* "Nano-scale traceable magnetic field measurements", a joint research project funded by the European Metrology Programme for Innovation and Research (EMPIR).

A. Manzin is with the Istituto Nazionale di Ricerca Metrologica (INRIM), Torino, 10135 Italy (e-mail: a.manzin@inrim.it).

V. Nabaei is with the Department of Electrical Engineering, Islamic Azad University, Hidaj Branch, Hidaj, 45731 Iran (e-mail: vahid.nabaei@gmail.com).

R. Ferrero is with the Istituto Nazionale di Ricerca Metrologica (INRIM), Torino, 10135 Italy, and with the Politecnico di Torino, Torino, 10129 Italy (e-mail: r.ferrero@inrim.it).

bead number is heavily influenced by the magnetostatic dipolar interactions between beads. We also find that the signal can deviate from linearity, due to the spatial non-uniformity in the device response. In particular, a possible enhancement of sensitivity can be obtained when beads are located not over the central part of the Hall cross, but towards its corners. All these conclusions are supported by a detailed parametric analysis, where external field amplitude, device dimension, bead number, interbead distance, bead vertical position and size of the area occupied by the bead ensemble are varied.

II. NUMERICAL MODEL

The voltage response of semiconductor Hall devices to the stray field of an ensemble of superparamagnetic nanobeads is simulated by means of a 2D finite element code, which enables to calculate the spatial distribution of the electric potential inside the Hall plate under the assumptions of diffusive transport regime and non-uniform magnetic field [8, 20]. In the implemented model, the electron transport is described by means of a spatially dependent conductivity tensor $\vec{\sigma}$ with elements

$$\begin{cases} \sigma_{xx} = \sigma_{yy} = \dfrac{\sigma_0}{1+\left[\mu B_z(x,y)\right]^2} \\ \sigma_{xy} = -\sigma_{yx} = \mu B_z(x,y)\sigma_{xx} \end{cases} \quad (1)$$

where $B_z(x,y)$ is the z-component of the magnetic field in the device plane (x,y), σ_0 is the zero-field electrical conductivity and μ is the electron mobility [21-23]. By expressing the electric field $\mathbf{E}$ as a function of scalar potential ϕ ($\mathbf{E} = -\nabla\phi$) and considering the equation of continuity for current density vector $\mathbf{J}$, it results that

$$\nabla\cdot\left[\vec{\sigma}(x,y)\nabla\phi(x,y)\right] = 0 \quad (2)$$

The problem definition is completed by the following boundary conditions

$$\mathbf{J}\cdot\mathbf{n} = 0 \text{ on insulating boundaries;}$$
$$\int_{S_i}\mathbf{J}\cdot\mathbf{n}ds = I_i \text{ on } i\text{-th current contact with injected current } I_i. \quad (3)$$

Once solved (2), the Hall voltage is evaluated as the difference between the values of the electric potential at the two voltage contacts. These are handled as floating electrodes with uniform unknown potential, introducing an integral constraint that ensures that current density vector is divergence-free.

The detection mechanism here modeled is based on the ac-dc Hall magnetometry technique [24, 27]. Specifically, the magnetic field in (1) incorporates a uniform external field, directed orthogonally to the device surface and composed of a dc signal, governing the bead magnetization alignment, and a small ac excitation, i.e. $\mathbf{B}_{ext}=\mathbf{B}_{dc}+\mathbf{B}_{ac}$. Moreover, it includes the z-component of the stray field produced by an ensemble of N superparamagnetic nanobeads, arranged in a 2D array located at distance h above the device active surface, as schematized in Fig. 1(a). Each bead, having volume V_{bead}, is an aggregate of nanoparticles with magnetic moment μ_{nano} and average volume V_{nano}. The beads, supposed to be uniformly magnetized along the direction of $\mathbf{B}_{ext} = B_{ext}\mathbf{k}$ and represented as magnetic dipoles whose magnetic moment obeys Langevin function, are responsible for the generation of a field whose z-component is

$$B_{beads_z}(x,y) = \frac{\mu_0}{4\pi}\sum_{k=1}^{N} m_k(B_{ext})\left(\frac{3h^2}{r_k^5}-\frac{1}{r_k^3}\right) \quad (4)$$

where r_k is the distance between the point of calculus and the barycentre of the k-th nanobead with magnetic moment amplitude m_k [27].

Following the ac-dc Hall magnetometry technique, the Hall voltage can be decomposed into a dc and an ac term, which can be in turn separated into two contributions, one deriving from the only applied external field and the other from the stray field of the magnetized beads. When sweeping the dc field in the absence of beads, the ac Hall voltage does not change; when the beads are present, the ac signal varies in dependence on the number and magnetic susceptibility of the beads. To mimic the ac-dc detection scheme, the resolution of bead magnetic moments is estimated by calculating the amplitude (peak value) of the ac Hall voltage due to bead ensemble, $\hat{V}_{ac,beads}$, as a function of dc field. To extrapolate the ac contribution, we approximate m_k in the following way

$$m_k(B_{ext}) \cong m_k\left(B_{k,z}(B_{dc})\right) + B_{ac}\frac{V_{bead}}{\mu_0}\chi_k\left(B_{k,z}(B_{dc})\right) \quad (5)$$

where χ_k is the magnetic susceptibility of the k-th nanobead, given by

$$\chi_k(B_{k,z}) = \frac{\mu_0\mu_{nano}^2}{k_B T V_{nano}}\left\{\left(\frac{k_B T}{\mu_{nano}B_{k,z}}\right)^2 - \left[\sinh\left(\frac{\mu_{nano}B_{k,z}}{k_B T}\right)\right]^{-2}\right\} \quad (6)$$

with k_B being the Boltzmann constant and T the absolute temperature [20]. In (5), $B_{k,z}$ is the z-component of the magnetic field seen by the k-th bead, which is the sum of the external source B_{dc} (considering the approximation introduced to derive the ac contribution) and the field generated by all the other beads, i.e.

$$\mathbf{B}_k = \mathbf{B}_{dc} + \frac{\mu_0}{4\pi}\sum_{n=1,n\neq k}^{N}\left[\frac{3(\mathbf{m}_n\cdot\mathbf{r}_{nk})\mathbf{r}_{nk}}{r_{nk}^5} - \frac{\mathbf{m}_n}{r_{nk}^3}\right] \quad (7)$$

where $\mathbf{r}_{nk}$ is the vector from the n-th to the k-th bead, as schematized in Fig. 1(b). The bead magnetic moments are

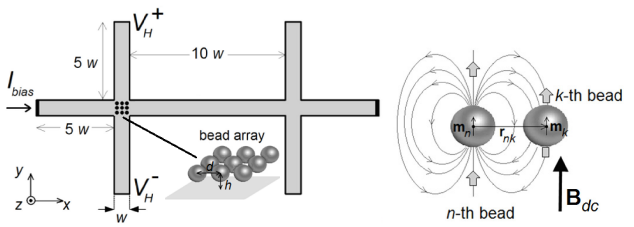

(a) (b)

Fig. 1. (a) Scheme of the considered double-cross Hall sensor with representation of the 2D array of superparamagnetic nanobeads immobilized above the device surface. (b) Scheme of the magnetostatic interaction between two adjacent beads.

obtained through a relaxation based iterative method, starting from the following estimation

$$\mathbf{m}_{k,0} = \mu_{nano} \frac{V_{bead}}{V_{nano}} L\left(\frac{\mu_{nano}\mathbf{B}_{dc}}{k_B T}\right) \tag{8}$$

being $L(.)$ the Langevin function. At the i-th iteration, the magnetic moment of the k-th bead is updated as

$$\mathbf{m}_{k,i} = \mathbf{m}_{k,i-1} - \lambda\left[\mathbf{m}_{k,i-1} - \mu_{nano} \frac{V_{bead}}{V_{nano}} L\left(\frac{\mu_{nano}\mathbf{B}_{k,i-1}}{k_B T}\right)\right] \tag{9}$$

with relaxation constant $\lambda \sim 1$ [28].

The developed finite element model was proven to be reliable under different operative conditions, being already validated by comparison to experimental results in various applications of miniaturized Hall sensors. In particular, it was previously used in the detection of a single magnetic microbead [8] and in the calibration of magnetic tips via scanning gate microscopy technique [23, 29].

III. Parametric Analysis

In this Section, the developed numerical model is applied to investigate the performance of micro-Hall sensors, when used for the detection and quantification of an ensemble of magnetic nanobeads. The aim is to study the influence on device sensitivity, signal proportionality to bead number and signal linearity of different parameters, i.e. external dc field, device dimension, bead number, interbead distance, bead vertical position and size of the area occupied by the beads. As an output, we calculate the amplitude of the ac Hall voltage due to the bead ensemble ($\hat{V}_{ac,beads}$).

A. Simulation Parameters

The attention is focused on InSb Hall plates composed of two symmetric crosses, with thickness of 300 nm and width w in the micrometer range (w = 1 μm if not differently specified). As depicted in Fig. 1(a), the length of the current arm and of the transverse voltage arms is assumed equal to $22w$ and $5w$, respectively. The InSb film has a carrier concentration of $3.9 \cdot 10^{16}$ cm^{-3} and an electron mobility of 1.3 m^2/Vs [13, 30] (the estimated voltage-noise spectral density is

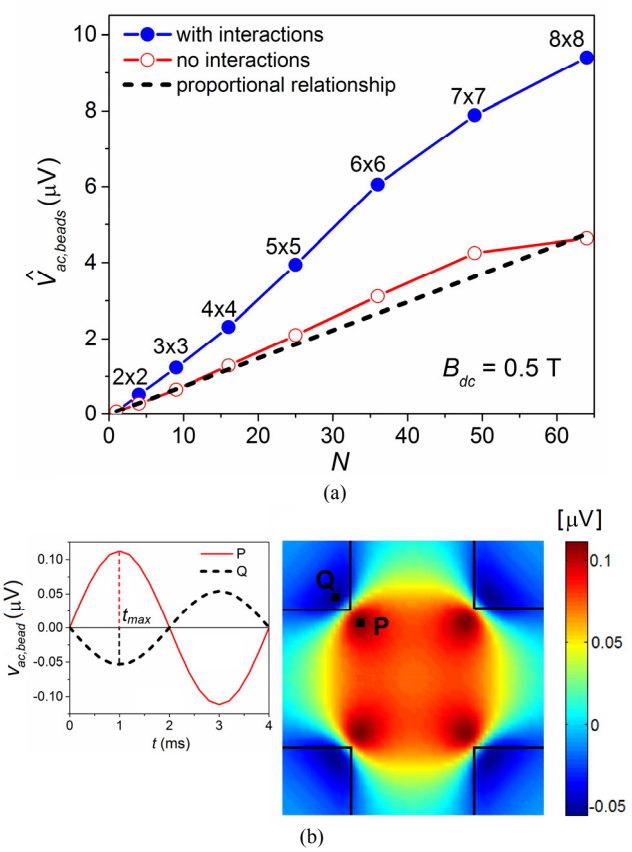

Fig. 2. (a) Amplitude of the ac Hall voltage due to bead array versus bead number N: comparison of the signals obtained with and without bead interactions to the "ideal" proportional relationship (B_{dc} = 0.5 T). The probe width is fixed to 1 μm, the interbead distance to 160 nm and the height of bead array to 100 nm. (b) Map of the corresponding instantaneous ac Hall voltage due to a bead placed in different grid points of the Hall cross. The map reports the signal calculated at the time instant corresponding to the peak value of B_{ac}. The graph on the left shows the time dependence of the ac Hall voltage due to a single bead, when the bead is located in proximity to the top left cross corner, above the device active area (point P) or above the region outside (point Q).

~12.2 nV/√Hz). The device is biased by a dc current of 40 μA (the corresponding minimal detectable field is ~0.57 μT/√Hz); the amplitude and frequency of the ac magnetic field are fixed to 10 mT and 250 Hz, respectively, whereas B_{dc} is varied.

The Hall signal is investigated under the presence of a monolayer of N equal superparamagnetic nanobeads. These are arranged in a square array immobilized at a vertical height h from the active sensing area, at the intersection of current and voltage arms, and with interbead (center-to-center) distance d. If not differently specified, parameters h (distance from bead barycentres to device top surface) and d are fixed to 100 nm and 160 nm, respectively. The nanobeads, with spherical shape and diameter of 150 nm, are aggregates of close-packed fcc FePt nanoparticles with average diameter of 3 nm and magnetic moment of 2700 μ_B [13, 31].

B. Influence of Bead Number

The influence of bead number N on the device response is investigated by comparing the "real" signal to the one obtained disregarding magnetostatic interactions between

beads and to the "ideal" proportional relationship. The "real" signal is calculated by including bead interactions and the effects related to bead position with respect to the device active area, following the complete modeling procedure described in Section II. The second one is obtained by approximating the magnetic field observed by the *k*-th bead, namely $\mathbf{B}_k$ in (7), as $\mathbf{B}_{dc}$. In this way, we exclude the magnetostatic interactions between beads, but we take into account the relevant information about the location of bead array. The "ideal" proportional relationship is extrapolated by multiplying the amplitude of the ac Hall voltage due to a single bead located at the cross center by *N*. In this way, we exclude simultaneously the effects of interbead magnetostatic interactions and non-uniformity in the device response, associated with bead array position.

The comparison among the three estimations of $\hat{V}_{ac,beads}$ as

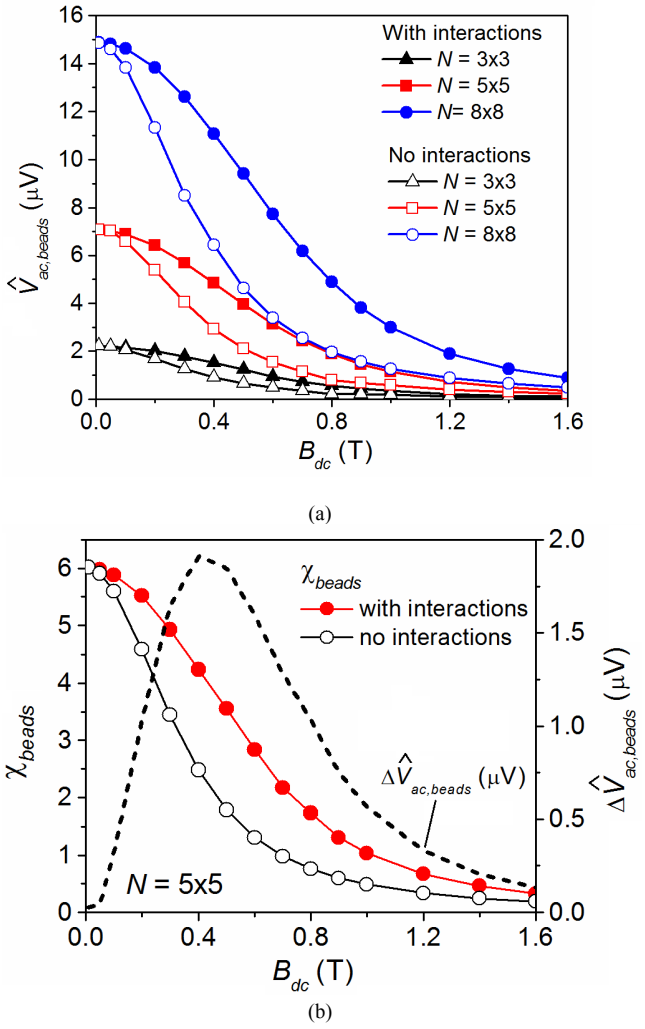

Fig. 3. (a) Amplitude of the ac Hall voltage due to bead array as a function of dc field and bead number *N*: comparison between the cases with and without bead interactions. The probe width is fixed to 1 μm, the interbead distance to 160 nm and the height of bead array to 100 nm. (b) Magnetic susceptibility versus dc field for a 5×5 bead array, considering and excluding bead interactions. On the same graph: corresponding variation in the ac Hall voltage due to the bead array, calculated as the difference between the values for the cases with and without interactions.

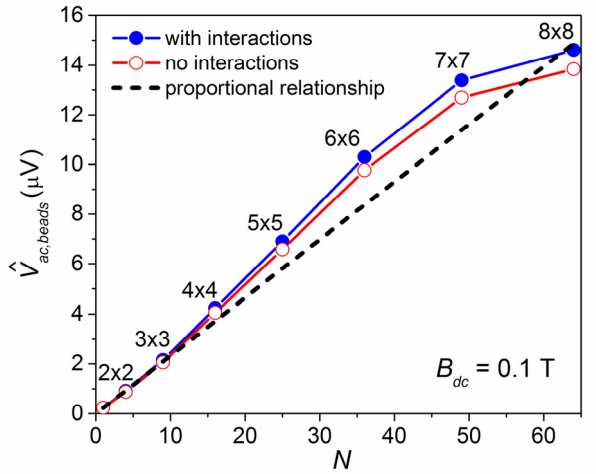

Fig. 4. Amplitude of the ac Hall voltage due to bead array versus bead number *N*: comparison of the signals obtained with and without bead interactions to the "ideal" proportional relationship (B_{dc} = 0.1 T). The probe width is fixed to 1 μm, the interbead distance to 160 nm and the height of bead array to 100 nm.

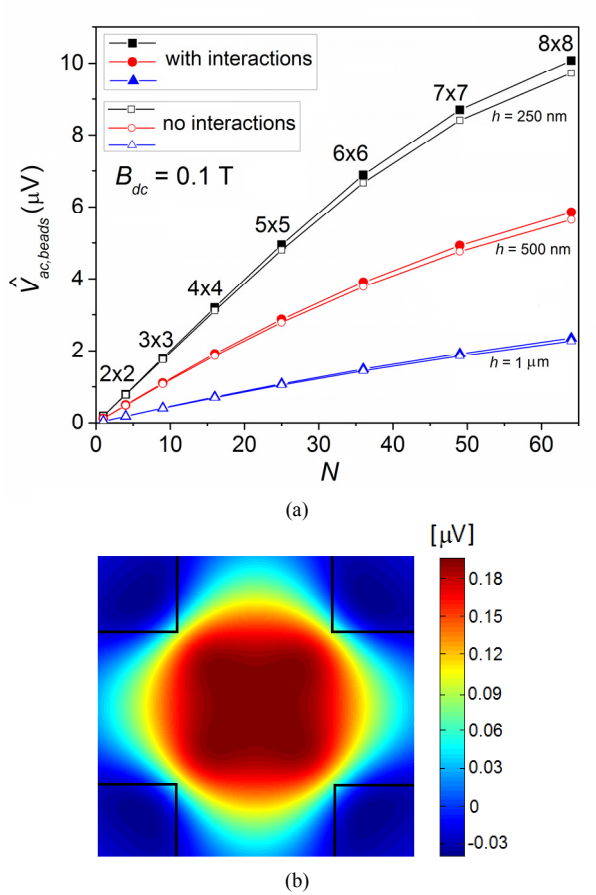

Fig. 5. (a) Amplitude of the ac Hall voltage due to bead array versus bead number *N*: comparison of the signals obtained with and without bead interactions varying the height *h* of bead array from 250 nm to 1 μm. The probe width is fixed to 1 μm, the interbead distance to 160 nm and the dc field to 0.1 T. (b) Map of the corresponding instantaneous ac Hall voltage due to a bead placed in different grid points of the Hall cross. The map reports the signal calculated at the time instant corresponding to the peak value of B_{ac} when *h* = 250 nm.

a function of bead number N is reported in Fig. 2(a). The results, obtained for B_{dc} = 0.5 T, put in evidence a strong deviation from the "ideal" proportional behavior of the "real" signal. The rate of increase is higher than N, showing a more rapid increment when the array is entirely located over the active sensing area (up to N = 6×6) and a change of slope for high numbers of beads (e.g., for N = 8×8), since in this case the array partially overlaps the active sensing area, interesting regions external to the Hall bar. The comparison to the signal calculated by disregarding bead interactions demonstrates that the deviation from the "ideal" proportional behavior (of a factor of about 2) is mainly a consequence of the magnetostatic dipole-dipole interactions between beads. These can lead to an erroneous estimation of the bead number; as an example, when N = 6×6 the "real" signal is practically the double of the proportional one, seeming to correspond to 72 beads and not to 36.

Moreover, there is a source of deviation from linearity, which is the spatial non-uniformity in the device response to the stray field of the beads. This is well demonstrated by Fig. 2(b), which reports the map of the instantaneous ac Hall voltage due to a single bead, placed in different grid points of the Hall cross. The signal is calculated at the time instant corresponding to the peak value of B_{ac}, extracting the contribution from the only bead stray field. If the bead is positioned over the Hall junction, the instantaneous ac Hall voltage reaches its maximum positive value, whereas if it is located outside the active sensing region, the signal is reversed [15, 32], and has an amplitude that tends to noise level. This change in behavior is illustrated by the graph on the left in Fig. 2(b).

The map of device sensitivity highlights a quite spatially homogeneous behavior in the central part of the Hall junction with peaks towards the cross corners, due to the local modification of the current path. This result, also found in Ref. [17], demonstrates why the curve for non-interacting beads deviates from the "ideal" proportional relationship.

C. *Influence of dc Magnetic Field*

The device response to the stray field generated by the nanobead ensemble can be finely tuned by varying the dc magnetic field B_{dc}.

We have verified that when maintaining the other parameters fixed, the dc excitation does not affect the spatial configuration of the 2D map of the ac Hall voltage signal. This means that the same spatial non-uniformity is found when sweeping B_{dc}. As an example, the peaks at the cross corners observed when the bead vertical position h is set at 100 nm [Fig. 2(b)] can be found in the entire range of variation of B_{dc}, apart from a change in the signal levels. Specifically, the peak values reduce from ~0.35 μV (~0.11 μV) to ~28 nV when B_{dc} is increased from to 0.1 T (0.5 T) to 1 T.

On the contrary, the contribution from bead magnetostatic interactions is strongly affected by B_{dc}, as shown in Fig. 3(a), which reports $\hat{V}_{ac,beads}$ versus B_{dc} for arrays composed of 3×3, 5×5 and 8×8 beads, comparing the cases with and without interactions. The stronger differences between the two behaviors are observed when B_{dc} ranges from ~0.2 T to ~1 T. In particular, the magnetostatic dipole-dipole interactions lead to a decrease in the local field acting on each bead; as an example, when B_{dc} = 1 T, the effective average field applied to a bead belonging to a 5×5 array is reduced to two-thirds. This diminution in the field acting on the beads affects the magnetic susceptibility of the array, producing a shift in the curve of $\chi_{beads}(B_{dc})$ towards higher values of B_{dc} or, in other terms, the amplification of χ_{beads} at a specific value of B_{dc} [Fig. 3(b)]. As a consequence, there is an increment of $\hat{V}_{ac,beads}$ with respect to the case in which bead interactions are disregarded, since the voltage signal is proportional to $\chi_{beads}(B_{dc})$. In particular, the difference between the values of $\hat{V}_{ac,beads}$ calculated with and without interactions is proportional to $\partial\chi_{beads}(B_{dc})/\partial B_{dc}$, where $\chi_{beads}(B_{dc})$ is estimated by including bead interactions. For the case of the 5×5 array, the strongest effect of magnetostatic interactions is found for B_{dc} ~0.4 T, whereas it becomes negligible when B_{dc} tends to zero, as demonstrated by Fig. 3(b).

As shown by Fig. 3(a) the condition $B_{dc} \rightarrow 0$ leads to a reduction in the impact of bead magnetostatic interactions as well as to an increase in the ac Hall voltage signal. A decrease in the effects of bead interaction can be also found for large values of dc field, but at the cost of a strong detriment of the device response. For very large dc fields (e.g. $B_{dc} > 1.6$ T), the considered magnetic beads reach saturation and their magnetic susceptibility becomes nearly zero. This means that the additional ac field excitation has negligible influence on the bead magnetic moments and the total ac Hall voltage signal is practically the same as if no beads are present, as clearly stated in Ref. [14]. Thus, for $B_{dc} > 1.6$ T, the ac signal due the only stray field of the beads (obtained extracting the contribution from the excitation) tends to zero.

It is also interesting to notice that the decrease in the local effective field applied to each bead, caused by bead magnetostatic interactions, produces an effect similar to the addition of a fictitious temperature to the actual temperature T in the Langevin function argument. This approach was proposed in Refs. [33, 34] as a phenomenological model to describe interparticle interactions. The fictitious increase in T and the "apparent" decrease in B_{dc} (due to the overlapping of the opposite stray field generated by the interacting beads) have similar consequences on the bead magnetic moment, since T is at the denominator of the Langevin function argument, while B_{dc} is at the numerator.

Finally, the proportionality of the device response to bead number can be controlled by changing the dc field that is applied to magnetize the beads. This is well demonstrated by the comparison of Fig. 2(a) to Fig. 4, which reports the "real" signal, the one obtained disregarding magnetostatic interactions and the "ideal" proportional relationship as a function of bead number N, when B_{dc} = 0.1 T. It is evident that the decrease in B_{dc} reduces the impact of magnetostatic interactions, leading to a more proportional signal to N.

As a conclusion of the above analysis, the "ideal" proportionality to N can be practically found when B_{dc} is lower than 50 mT. This is in line with the results reported in Ref. [19], where the degree of accuracy of the bead number detection is evaluated at zero dc magnetic field, showing an overall proportional behavior versus N. Anyway, a non-zero dc field is typically applied to discriminate between the stray field of the beads and possible spurious signals.

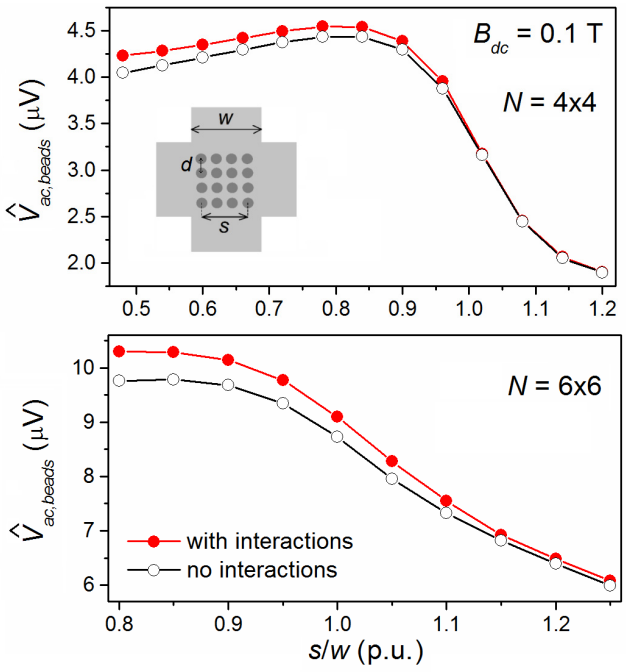

Fig. 6. Amplitude of the ac Hall voltage due to bead array versus the ratio of the size s of the area occupied by the array to the Hall cross width w for N equal to (a) 4×4 and (b) 6×6, considering B_{dc} = 0.1 T. The probe width is fixed to 1 μm, the height of bead array to 100 nm and the interbead distance is varied with s.

D. *Influence of Bead Distance from Sensor Surface*

The effect of vertical position of bead array has been investigated by varying parameter h, i.e. the distance from bead barycentres to device top surface, from 100 nm up to 1 μm. In the analysis the dc field is set at 0.1 T.

As shown in Fig. 5, the increase in h leads to a reduction in non-uniformity in the sensor response, giving rise to a more linear signal versus bead number N. Contrarily to h = 100 nm (Fig. 4), when h = 1 μm the signal linearity is preserved also for very high values of N, without deflection from N > 49. However, the increase in h leads to a strong detriment of the signal, e.g. for N = 64 $\hat{V}_{ac,beads}$ diminishes from to 14.6 μV (10 μV) to 2.4 μV, when h is varied from to 100 nm (250 nm) to 1 μm. Moreover, when h = 1 μm the signal reaches noise level for low numbers of beads.

The reduction in non-uniformity in the sensor response due to the increase in h is well evidenced by Fig. 5(b), which shows the device sensitivity as a function of the in-plane position of a single bead, located at a height of 250 nm. In comparison with the map of Fig. 2(b), calculated for h = 100 nm, the peaks at the cross corners almost disappear. In particular, the device response is characterized by a uniform behavior over the active area, with a central plateau region, whose extension increases with h, at the cost of a conspicuous signal reduction.

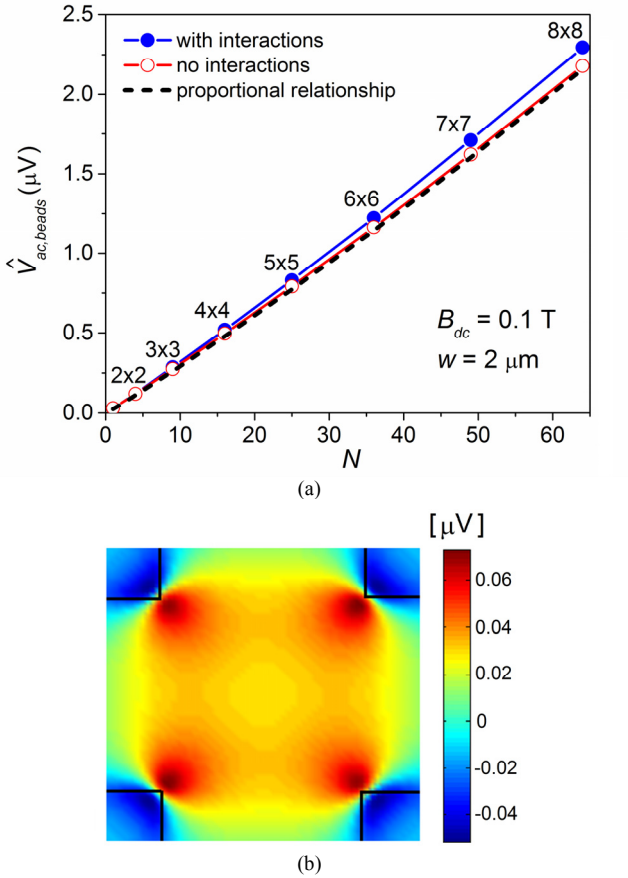

Fig. 7. (a) Amplitude of the ac Hall voltage due to bead array versus bead number N: comparison of the signals obtained with and without bead interactions to the "ideal" proportional relationship for probe width w equal to 2 μm. The dc field is 0.1 T, the interbead distance is 160 nm and the height of bead array is 100 nm. (b) Map of the corresponding instantaneous ac Hall voltage due to a bead placed in different grid points of the Hall cross. The map reports the signal calculated at the time instant corresponding to the peak value of B_{ac}.

E. *Influence of Interbead Distance and Size of Area Occupied by Beads*

We have also analyzed the role of interbead distance d for different values of bead number N, by changing parameter s/w, i.e. the ratio of the size s of the area occupied by the bead array to the Hall cross width w. Specifically, parameter s/w, depicted in the inset of Fig. 6(a), is varied from 0.48 (d = 160 nm) to 1.2 (d = 400 nm) when N = 4×4; whereas, it is varied from 0.8 (d = 160 nm) to 1.25 (d = 250 nm) when N = 6×6. The dc field is fixed to 0.1 T.

For the cases with N equal to 4×4 or lower, there is an important contribution from spatial non-uniformity in the device response, as confirmed by the strong non-monotonic

behavior of $\hat{V}_{ac,beads}$ versus s/w [Fig. 6(a)]. In particular, there is an initial amplification of the signal at the increase in s/w, since the bead array tends towards an arrangement where part of the beads at the periphery are located in proximity to the cross corners, where a peak in the device response is found. Moreover, when the size of the array is comparable to w or higher (d > 330 nm), magnetostatic interactions become negligible and the values of $\hat{V}_{ac,beads}$ estimated with and without interactions almost coincide.

For high values of N (e.g., 6×6), the effects of spatial non-uniformity in the device response are very weak and, overall, the signals decrease with s/w. On the contrary, as illustrated by Fig. 6(b), magnetostatic interactions still provide an important contribution also when s/w ~1, being the interbead distance d equal to 200 nm.

F. Influence of Device Size

Finally, we have studied the impact of magnetostatic interactions between beads for a larger Hall cross (cross width w = 2 μm), comparing the signals obtained with and without interactions to the "ideal" proportional relationship, as shown in Fig. 7(a). The results are determined for a dc field of 0.1 T; for a comparison, the corresponding curves calculated with w = 1 μm are reported in Fig. 4.

For the 2 μm width device, due to the decrease in the bead-sensor coupling, the deviation from the "expected" proportional behavior is strongly reduced at the cost of a lower magnetic moment resolution. Moreover, the effects of spatial non-uniformity in the device response become negligible, as evident from the relative map of the instantaneous ac Hall voltage due to a bead placed in different grid points of the Hall cross, shown in Fig. 7(b). For the 2 μm width device the area characterized by uniform response is larger than the one occupied by a 8×8 bead array with interbead distance d = 160 nm.

IV. CONCLUSION

The present study has investigated the possibility of using micrometer semiconductor Hall devices as magnetic nanobead counters, which adopt the ac-dc magnetometry technique. The analysis has been performed by considering an InSb double-cross Hall sensor and a 2D array of beads (aggregates of FePt nanoparticles), immobilized over the active sensing area with different interbead distance.

The study has demonstrated that a deviation of the Hall voltage signal from proportionality to the bead number can be obtained under specific operative conditions. A possible source of deviation from the "ideal" proportional behavior is represented by the magnetostatic interactions between beads, which can lead to an amplification of the global magnetic susceptibility and, thus, to an enhancement of the signal with a rate of increase higher than the bead number. Another critical aspect, which can cause loss of signal linearity, is connected with the spatial non-uniformity of the magnetic moment resolution, due to the enhancement of sensitivity at the Hall cross corners.

It has been observed that the deviation from proportionality can be reduced by operating at low dc magnetic fields (below 0.1 T), where the effects of bead magnetostatic interactions are weaker. Another mean to gain proportionality in the device response is the usage of Hall crosses with a larger sensing area, but at the cost of a reduction in the voltage signal. Moreover, the loss of linearity due to spatial non-uniformity of sensitivity can be controlled by increasing the distance of the bead array from the sensor surface. However, this leads to a strong detriment of the signal, which can reach noise level for low numbers of beads.

In conclusion, the effects of dc field and size of the device active area have to be carefully taken into account in the design of miniaturized Hall sensors employable as bead counters for lab-on-chip applications.

REFERENCES

[1] G. Boero, M. Demierre, P. A. Besse, and R. S. Popovic, "Micro-Hall devices: performance, technologies and applications", *Sensors and Actuators A: Physical*, vol. 106, pp. 314–320, 2003.

[2] J. Lenz and A. S. Edelstein, "Magnetic Sensors and Their Applications", *IEEE Sensors Journal*, vol. 6, pp. 631-649, 2006.

[3] H. Xu, L. Huang, Z. Zhang, B. Chen, H. Zhong, and L.-M. Peng, "Flicker noise and magnetic resolution of graphene Hall sensors at low frequency", *Appl. Phys. Lett*., vol. 103, 112405, 2013.

[4] J. Llandro, J. J. Palfreyman, A. Ionescu, and C. H. W. Barnes, "Magnetic biosensor technologies for medical applications: a review", *Med. Biol. Eng. Comput*., vol. 48, pp. 977-998, 2010.

[5] P. Manandhar, K. S. Chen, K. Aledealat, G. Mihajlović, C. S. Yun, M. Field, G. J. Sullivan, G. F. Strouse, P. B. Chase, S. von Molnár, and P. Xiong, "The detection of specific biomolecular interactions with micro-Hall magnetic sensors", *Nanotechnology*, vol. 20, 355501, 2009.

[6] C. R. Tamanaha, S. P. Mulvaney, J. C. Rife, and L. J. Whitman, "Magnetic labeling, detection, and system integration", *Biosensors and Bioelectronics*, vol. 24, pp. 1-13, 2008.

[7] T. Takamura, P. J. Ko, J. Sharma, R. Yukino, S. Ishizawa, and A. Sandhu, "Magnetic-Particle-Sensing Based Diagnostic Protocols and Applications", *Sensors*, vol. 15, pp. 12983-12998, 2015.

[8] A. Manzin, E. Simonetto, G. Amato, V. Panchal, and O. Kazakova, "Modeling of graphene Hall effect sensors for microbead detection", *J. Appl. Phys.*, vol. 117, 17B732, 2015.

[9] D. Issadore, Y. I. Park, H. Shao, C. Min, K. Lee, M. Liong, R. Weissleder, and H. Lee, "Magnetic sensing technology for molecular analyses", *Lab Chip*., vol. 14, pp. 2385–2397, 2014.

[10] A. Sandhu, H. Handa, and M. Abe, "Synthesis and applications of magnetic nanoparticles for biorecognition and point of care medical diagnostics", *Nanotechnology*, vol. 21, 442001, 2010.

[11] Q. A. Pankhurst, J. Connolly, S. K. Jones, and J. Dobson, "Applications of magnetic nanoparticles in biomedicine", *J. Phys. D: Appl. Phys*., vol. 36, pp. R167–R181, 2003.

[12] K. Togawa, H. Sanbonsugi, A. Sandhu, M. Abe, H. Narimatsu, K. Nishio, and H. Handa, "Detection of magnetically labeled DNA using pseudomorphic AlGaAs/InGaAs/GaAs heterostructure micro-Hall biosensors", *J. Appl. Phys*., vol. 99, 08P103, 2006.

[13] L. Di Michele, C. Shelly, J. Gallop, and O. Kazakova, "Single particle detection: phase control in submicron Hall sensors", *J. Appl. Phys*., vol. 108, 103918, 2010.

[14] M. S. Gabureac, L. Bernau, G. Boero, and I. Utke, "Single Superparamagnetic Bead Detection and Direct Tracing of Bead Position Using Novel Nanocomposite Nano-Hall Sensors", *IEEE Transactions on Nanotechnology*, vol. 12, pp. 668-673, 2013.

[15] K. Aledealat, G. Mihajlović, K. Chen, M. Field, G. J. Sullivan, P. Xiong, P. B. Chase, and S. von Molnár, "Dynamic micro-Hall detection of superparamagnetic beads in a microfluidic channel", *J. Magn. Magn. Mat.*, vol. 322, pp. L69-L72, 2010.

[16] K. Togawa, H. Sanbonsugi, A. Lapicki, M. Abe, H. Handa, and A. Sandhu, “High-sensitivity InSb thin-film micro-Hall sensor arrays for simultaneous multiple detection of magnetic beads for biomedical applications”, *IEEE Trans. Magn*., vol. 41, pp. 3661-3663, 2005.

[17] Y. Kumagai, Y. Imai, M. Abe, S. Sakamoto, H. Handa, and A. Sandhu, “Sensitivity dependence of Hall biosensor arrays with the position of superparamagnetic beads on their active regions”, *J. Appl. Phys*., vol. 103, 07A309, 2008.

[18] K. Skucha, S. Gambini, P. Liu, M. Megens, J. Kim, and B. E. Boser, “Design Considerations for CMOS-Integrated Hall-Effect Magnetic Bead Detectors for Biosensor Applications”, *J. Microelectromech. Syst*., vol. 22, pp. 1327–1338, 2013.

[19] W. Lee, S. Joo, S. U. Kim, K. Rhie, J. Hong, K. Shin, and K. H. Kim, “Magnetic bead counter using a micro-Hall sensor for biological applications”, *Appl. Phys. Lett*., vol. 94, 153903, 2009.

[20] A. Manzin, V. Nabaei, and O. Kazakova, “Modelling and optimization of submicron Hall sensors for the detection of superparamagnetic beads”, *J. Appl. Phys*., vol. 111, 07E513, 2012.

[21] Y. G. Cornelissens and F. M. Peeters, “Response function of a Hall magnetosensor in the diffusive regime”, *J. Appl. Phys*., vol. 92, pp. 2006-2012, 2002.

[22] V. Nabaei, R. K. Rajkumar, A. Manzin, O. Kazakova, and A. Tzalenchuk, “Optimization of Hall bar response to localized magnetic and electric fields”, *J. Appl. Phys*., vol. 113, 064504, 2013.

[23] R. K. Rajkumar, A. Asenjo, V. Panchal, A. Manzin, Ó. Iglesias-Freire, and O. Kazakova, “Magnetic scanning gate microscopy of graphene Hall devices”, *J. Appl. Phys*., vol. 115, 172606, 2014.

[24] G. Mihajlović, K. Aledealat, P. Xiong, S. von Molnár, M. Field, and G. J. Sullivan, “Magnetic characterization of a single superparamagnetic bead by phase-sensitive micro-Hall magnetometry”, *Appl. Phys. Lett*., vol. 91, 172518, 2007.

[25] G. Mihajlović, P. Xiong, S. von Molnár, K. Ohtani, H. Ohno, M. Field, and G. J. Sullivan, “Detection of single magnetic bead for biological applications using an InAs quantum-well micro-Hall sensor”, *Appl. Phys. Lett*., vol. 87, 112502, 2005.

[26] L. Di Michele, C. Shelly, P. de Marco, P. See, D. Cox, and O. Kazakova, “Detection and susceptibility measurements of a single Dynal bead”, *J. Appl. Phys*., vol. 110, 063916, 2011.

[27] P. A. Besse, G. Boero, M. Demierre, V. Pott, and R. Popovic, “Detection of a single magnetic microbead using a miniaturized silicon Hall sensor”, *Appl. Phys. Lett*., vol. 80, pp. 4199-4201, 2002.

[28] B. B. Yellen and G. Friedman, “Analysis of repulsive interactions in chains of superparamagnetic colloidal particles for magnetic template-based self-assembly”, *J. Appl. Phys*., vol. 93, pp. 8447-8449, 2003.

[29] V. Panchal, H. Corte-León, B. Gribkov, L. A. Rodriguez, E. Snoeck, A. Manzin, E. Simonetto, S. Vock, V. Neu, and O. Kazakova, “Calibration of multi-layered probes with low/high magnetic moments”, *Scientific Reports*, vol. 7, 7224, 2017.

[30] T. Zhang, J. J. Harris, W. R. Branford, Y. V. Bugoslavsky, S. K. Clowes, L. F. Cohen, A. Husmann, and S. A. Solin, “Tuning the inherent magnetoresistance of InSb thin films”, *Appl. Phys. Lett*., vol. 88, 012110, 2006.

[31] L. Hao, C. Aßmann, J. C. Gallop, D. Cox, F. Ruede, O. Kazakova, P. Josephs-Franks, D. Drung, and T. Schurig, “Detection of single magnetic nanobead with a nano-superconducting quantum interference device”, *Appl. Phys. Lett*., vol. 98, 092504, 2011.

[32] S. M. Hira, K. Aledealat, K.-S. Chen, M. Field, G. J. Sullivan, P. B. Chase, P. Xiong, S. von Molnár, and G. F. Strouse, “Detection of Target ssDNA Using a Microfabricated Hall Magnetometer with Correlated Optical Readout”, *Journal of Biomedicine and Biotechnology*, vol. 2012, 492730, 2012.

[33] P. Allia, M. Coïsson, P. Tiberto, F. Vinai, M. Knobel, M. A. Novak, and W. C. Nunes, “Granular Cu-Co alloys as interacting superparamagnets”, *Phys. Rev. B*, vol. 64, 144420, 2001.

[34] J. M. Vargas, W. C. Nunes, L. M. Socolovsky, M. Knobel and D. Zanchet, “Effect of dipolar interaction observed in iron-based nanoparticles”, *Phys. Rev. B*, vol. 72, 184428, 2005.